Three-dimensional Reconstruction of a Co-complex of F-actin with Antibody Fab Fragments to Actin's NH_2 Terminus

Albina Orlova, Xiong Yu, and Edward H. Egelman
Department of Cell Biology and Neuroanatomy, University of Minnesota Medical School, Minneapolis, Minnesota 55455

ABSTRACT We have decorated F-actin with Fab fragments of antibodies to actin residues 1–7. These antibody fragments do not strongly affect the rigor binding of myosin S-1 to actin, but do affect the binding of S-1 to actin in the presence of nucleotide (DasGupta, G., and E. Reisler. 1989. *J. Mol. Biol.* 207:833–836; 1991. *Biochemistry.* 30:9961–9966; 1992. *Biochemistry.* 31:1836–1841). Although the binding constant is rather low, we estimate that we have achieved about 85% occupancy of the actin sites. Three-dimensional reconstructions from electron micrographs of both negatively stained and frozen-hydrated filaments show that the Fab fragment is bound at the location of the NH_2 terminus in the model of Holmes et al. (Holmes, K.C., D. Popp, W. Gebhard, and W. Kabsch. 1990. *Nature.* 347:37–44) for F-actin, excluding very different orientations of the actin subunit in the filament. Most of the mass of the antibody is not visualized, which is due to the large mobility of the NH_2 terminus in F-actin, differences in binding angle within the polyclonal antibody population, or a combination of both of these possibilities.

INTRODUCTION

Our understanding of the structural basis for actin's key role in muscle, cell motility and the maintenance of cell shape and form has been greatly advanced by an atomic structure for G-actin (Kabsch et al., 1990) and a model for the orientation of this subunit in F-actin (Holmes et al., 1990). An alternate model for F-actin (Schutt et al., 1993) has recently been advanced that is very different from the model of Holmes et al. (1990). Electron microscopy can be used to distinguish between these models, and has an important function in further advancing our understanding in this area. We have already been able to use electron microscopy to visualize differences between real F-actin filaments and the atomic model (Orlova and Egelman, 1992), as well as in visualizing different conformational states of F-actin (Orlova and Egelman, 1992; Orlova and Egelman, 1993). In this paper, we extend our studies by employing electron microscopy and three-dimensional reconstruction techniques to visualize a co-complex of F-actin and Fab fragments of antibodies to the NH_2 terminus of actin (Miller et al., 1987; DasGupta and Reisler, 1989, 1991, 1992).

We have undertaken this study for four reasons. First, actin is one of the most highly conserved protein families in biology, with a much stronger tissue specificity than species specificity between different actin isoforms. The NH_2 terminus of actin, however, is the least conserved part of the molecule, with the primary coding difference for the different isoforms lying in the first 10 NH_2-terminal residues (Herman, 1993). It is therefore likely that the NH_2 terminus of actin will be the most important determinant in providing the tissue specificity for actin via the interaction of actin-binding proteins with these residues.

Second, the binding of this particular Fab fragment to F-actin has interesting properties. In the absence of nucleotide, there is no strong competition between this antibody and myosin S-1, whereas significant interference is observed in the presence of nucleotide (DasGupta and Reisler, 1989, 1991, 1992). This suggests either that the antibody induces a conformational change in actin, such that the rigor binding of myosin is relatively unaffected but the active ATP-dependent binding is affected, or that the a2ntibody blocks a site that is only involved in the active binding of myosin, but not the rigor binding.

Third, because the epitope of this antibody is known, the seven NH_2-terminal residues of actin, a co-complex of the antibody on F-actin allows one to test the validity of the Holmes et al. (1990) model at low resolution. And fourth, we would like to determine whether the bound antibody affects the filament dynamics, such as torsional disorder (Egelman et al., 1982; Egelman and DeRosier, 1992).

MATERIALS AND METHODS

Specimen preparation

Actin was prepared from rabbit skeletal muscle and was labeled with phalloidin and erythrosin-maleimide for spectroscopic studies by Dr. E. Prochniewicz in the laboratory of Dr. David Thomas (University of Minnesota). We are trying to coordinate our efforts, and thus are interested in the three-dimensional structure of the actual labeled filaments used for the spectroscopic experiments (Prochniewicz et al., manuscript in preparation). The Fab fragment of the antibodies to actin residues 1–7 was obtained from Dr. Emil Reisler (Miller et al., 1987). The negatively stained electron microscopic grids of F-actin decorated by the Fab were made in a manner similar to that described by Craig et al. (1980) for thin filaments decorated with heavy mero myosin. All procedures were performed at room temperature. One drop (3 μl) of 1 μM F-actin was applied to a 300-mesh copper grid (coated with carbon film) for 1–2 min and rinsed off with 1–3 drops of F-actin buffer (50 mM KCl, 5 mM Tris-HCl, pH 7.8, 0.1 mM $CaCl_2$, 0.1 mM ATP). The last drop was replaced with 2–4 separate drops, each 6–10

Received for publication 6 August 1993 and in final form 9 November 1993.

Address reprint requests to Dr. Egelman, Dept. of Cell Biology and Neuroanatomy, 4-135 Jackson Hall, Univ. of Minnesota Medical School, 321 Church St. S.E., Minneapolis, MN 55455.

Dr. Orlova'a permanent address is Institute of Theoretical and Experimental Biophysics, Russian Academy of Sciences, Puschino, Russia.

0006-3495/94/02/276/10 $2.00

μl, of Fab at 3–6 μM in F-actin buffer. The last drop was left on the grid for 1–2 min and the grids were then rinsed with 3–4 drops of 1% (w/v) uranyl acetate.

Frozen-hydrated specimens for cryo-electron microscopy were prepared on a holey carbon film, using the same method of on-the-grid washing used with the antibody described previously. The samples were then rapidly frozen in a propane slush, and maintained at −170°C in a Gatan 626 (Pleasanton, CA) cold stage.

Electron microscopy

A JEOL 1200EXII, operating at an accelerating voltage of 120 kV, was used for all microscopy. The defocus was typically less than 0.5 μM for the negatively stained microscopy, and about 3.5 μM for the cryo-electron microscopy. The cryo-electron microscopy defocus was confirmed by examining the transform of a large (2048 × 2048 pixel) area of carbon film. Images used for reconstructions were recorded under minimal dose conditions, with no exposure to the beam at high magnification before recording. Images were recorded at approximately 30,000 × magnification, with the exact magnification determined from the 23 Å pitch helix of tobacco mosaic virus particles coprepared with the actin.

Image analysis

Electron micrographs were digitized with a 12-bit Eikonix photodiode camera, with a sampling of approximately 6 Å/pixel. Filament images were corrected for curvature (Egelman, 1986), padded into 128 × 2048 pixel arrays, and Fourier transformed. All transforms were performed on a Sky Warrior array processor, running on a VAX 3200. Layer lines were extracted from the transforms, and the near and far sides were averaged together. A reference layer line set, generated from a low-pass filtered version of the Holmes et al. (1990) model for F-actin, was used as a starting reference in searching for the translation, rotation, and polarity of each filament layer line set. After an initial average was calculated, this averaged layer line set was used as the new reference for the next cycle of alignment. This procedure was iterated three or four times, until there was no shift of individual filaments with respect to the average.

Statistical difference maps were computed as in Egelman and Yu (1989), with the addition that scale parameters α and β were chosen so that the total squared difference between the two maps,

$$\sum_{i=1}^{N_i}\sum_{j=1}^{N_j}[(\alpha\rho_1(i,j)+\beta)-\rho_2(i,j)]^2 \quad (1)$$

was at a minimum.

RESULTS

Incubation of F-actin filaments with the antibody fragment results in a clear binding of the antibody to F-actin (Fig. 1). The key problem in generating fully decorated filaments is the relatively low affinity of the antibody for actin, with an estimated binding constant of 7×10^5 M^{-1} (Miller et al., 1987). As one increases the concentration of the antibody with a fixed actin concentration, the background of unbound antibody also increases. In addition to using the procedure for on-the-grid decoration described in Materials and Methods, we have incubated 1 μM actin with 10 μM antibody. Based on the published binding constant, we estimate that under these conditions the occupancy of the antibody on actin is about 80–85%. The on-the-grid incubation method, which has been used for all the data in this paper, appears to result in at least this amount of binding, as judged by visual comparison of micrographs.

Fourier transforms of Fab-decorated actin filaments show a much greater background due to the large concentration of unbound Fab fragments surrounding the filaments. The transforms also show a large increase in the intensity of the first (1/350 Å) actin layer line, arising from the right-handed 700 Å pitch two-start helices (Fig. 1 *D*). This intensity increase can be clearly seen in the averaged layer lines (see Fig. 3). Examination of the transforms has also suggested that the first actin layer line may also be sharper in the Fab-decorated filaments. This is consistent with an apparent reduction in the

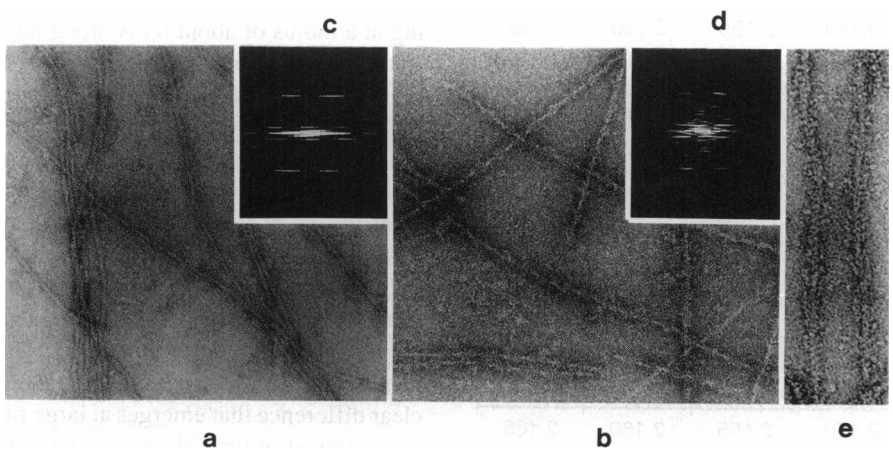

FIGURE 1 Electron micrograph of negatively stained actin-erythrosin-phalloidin filaments decorated with anti-actin Fab fragments (*b*), and control erythrosin-phalloidin-actin filaments (*a*). The relatively low affinity of the antibody for actin requires a large excess of the antibody, which accounts for the high background of antibody seen in the electron micrograph. Computed Fourier transforms of an Fab-decorated actin filament (*d*), and a control erythrosin-phalloidin-actin filament (*c*), after filament straightening. As with the images, the background is greatly increased in the transforms of Fab-decorated filaments (*d*), but the first actin layer line (at 1/351 Å) is also significantly strengthened and sharpened. In *e*, a higher magnification image is shown of two actin filaments incubated with a 1:1 molar ratio of the Fab fragments. This produces a much lower background, but also a lower occupancy. It can be seen that individual Fab fragments attach to the F-actin at different angles. The scale is provided in *a*, *b*, and *e* by the actin crossovers, which are variable, but have a mean of ~360 Å.

random angular disorder in actin filaments (Egelman et al., 1982; Egelman and DeRosier, 1992) induced by the Fab fragment binding. The axial spacing of the layer lines allows one to compute the average twist (in actin subunits per turn of the 59 Å pitch left-handed helix) for each filament. The variance of this distribution allows one to determine d_{rms}, the root mean square (rms) angular deviation per subunit within the filaments, from the relation (Stokes and DeRosier, 1987):

$$d_{rms} = \frac{2\pi\sigma_{upt}\sqrt{N}}{\langle upt \rangle^2} \quad (2)$$

where σ_{upt} is the standard deviation of the distribution of unit per turn values, N is the average number of subunits in each filament, and $\langle upt \rangle$ is the average twist in units per turn (about 2.157). For pure F-actin, we have measured an rms angular deviation of about 5.2° per subunit (Orlova and Egelman, 1992; Egelman and DeRosier, 1992), whereas the erythrosin-phalloidin-actin distribution shown in Fig. 2 suggests an rms angular deviation of about 3.5° per subunit, consistent with some reduction in angular disorder obtained with phalloidin. Measurements of variations in actin crossover spacings by Bremer et al. (1991) have also shown a similar effect of phalloidin on reducing this torsional disorder. With the Fab-actin complex, however, the distribution of units per turn suggests an rms angular disorder of about 1.9° per subunit. Thus, the Fab binding does appear to reduce the angular disorder in actin.

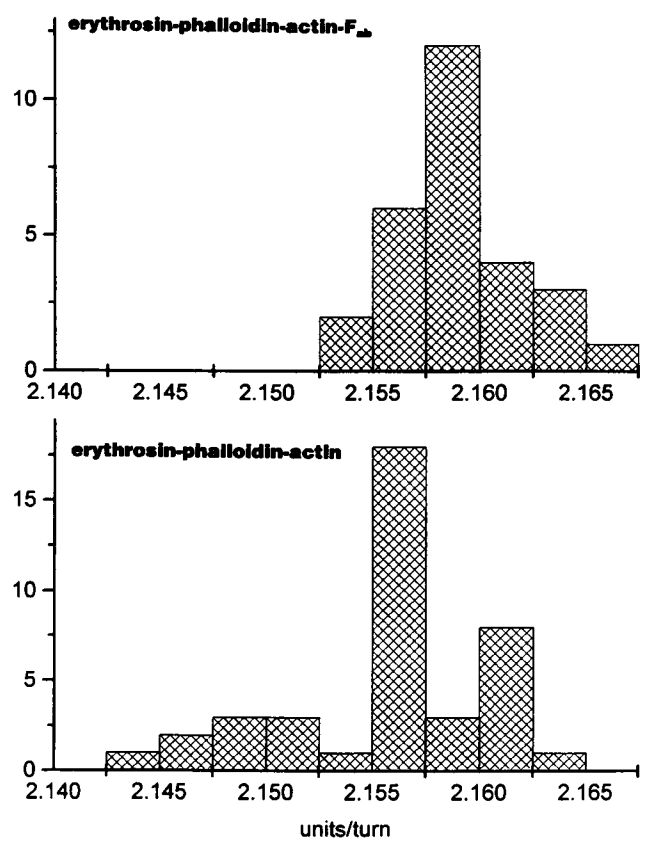

FIGURE 2 A comparison between the distribution of actin subunits per turn of the 59 Å pitch helix in Fab-decorated actin (*top*), and control erythrosin-phalloidin-actin filaments (*bottom*). The mean for the Fab-decorated filaments is 2.159 ± 0.0026 (SD), whereas the mean for the control filaments is 2.156 ± 0.0047 (SD). The reduced variance in the units per turn distribution seen with the Fab decoration is consistent with a reduction of the torsional disorder of subunits within those filaments.

Layer lines were extracted from the transforms of 21 control erythrosin-phalloidin-actin filaments and 26 Fab-decorated erythrosin-phalloidin-actin filaments. The layer lines and Bessel orders used were: $l = 0, n = 0$; $l = 1, n = 2$; $l = 2, n = 4$; $l = 5, n = -3$; $l = 6, n = -1$; $l = 7, n = 1$; $l = 8, n = 3$; and $l = 13, n = 0$. Filaments that did not average well together were excluded during iterative cycles of alignment of the individual filaments against an average, resulting in 18 filaments being retained in the final average for both the control and Fab-decorated filaments. One measure of how well filaments average together, as well as of the intrinsic polarity of the filaments, is the F-weighted phase residual averaged across all layer lines between an individual filament and the average. This can be computed for both possible polarities in which the filament is oriented against the average. For nonpolar filaments this phase residual would be the same for both orientations. The average phase residual for the Fab-decorated filaments was 53° for the proper polarity and 72° for the opposite polarity. The average phase residual for the control filaments was 45° for the proper polarity and 74° for the opposite polarity. These residuals are high, but reflect the poor signal to noise ratio. Further, although the helical disorder reflected by variations in layer-line spacing appears to be reduced, the antibodies appear to introduce a structural variation that can account for this increase in phase residual over the control. This is described below.

A comparison between the layer lines from control and Fab-decorated filaments (Fig. 3) shows a dramatic difference on the first layer line: a large peak appears in the Fab-decorated set at about 0.0075 $Å^{-1}$, indicative of contrast arising at a radius of about 65 Å along the two-start actin helix. Because this is beyond the radius of the actin filament, it strongly suggests that the Fab is binding to the filament.

The layer lines have been used to generate three-dimensional reconstructions, and contoured sections from these reconstructions are shown in Fig. 4, and rendered surfaces in Fig. 5. When the threshold density for the contours or surface is chosen so that 100% of the expected molecular volume for actin is enclosed, there is almost no visible contribution from the antibody. However, when this threshold value is reduced, so that ~195% of the expected actin molecular volume is enclosed (Figs. 4 *B* and 5 *B*), there is a very clear difference that emerges at large radius. Although we do not see most of the Fab mass even at this low contour level (the entire Fab mass would be about 20% greater than the actin mass), we interpret the additional mass that we do see to be the proximal portion of the Fab fragment. At this contour level, this high-radius feature has a volume of about 7500 $Å^3$, which corresponds to ~12% of the expected volume for a 50,000-mol wt Fab fragment. Given that we have used a contour level that yields ~167% of the expected actin

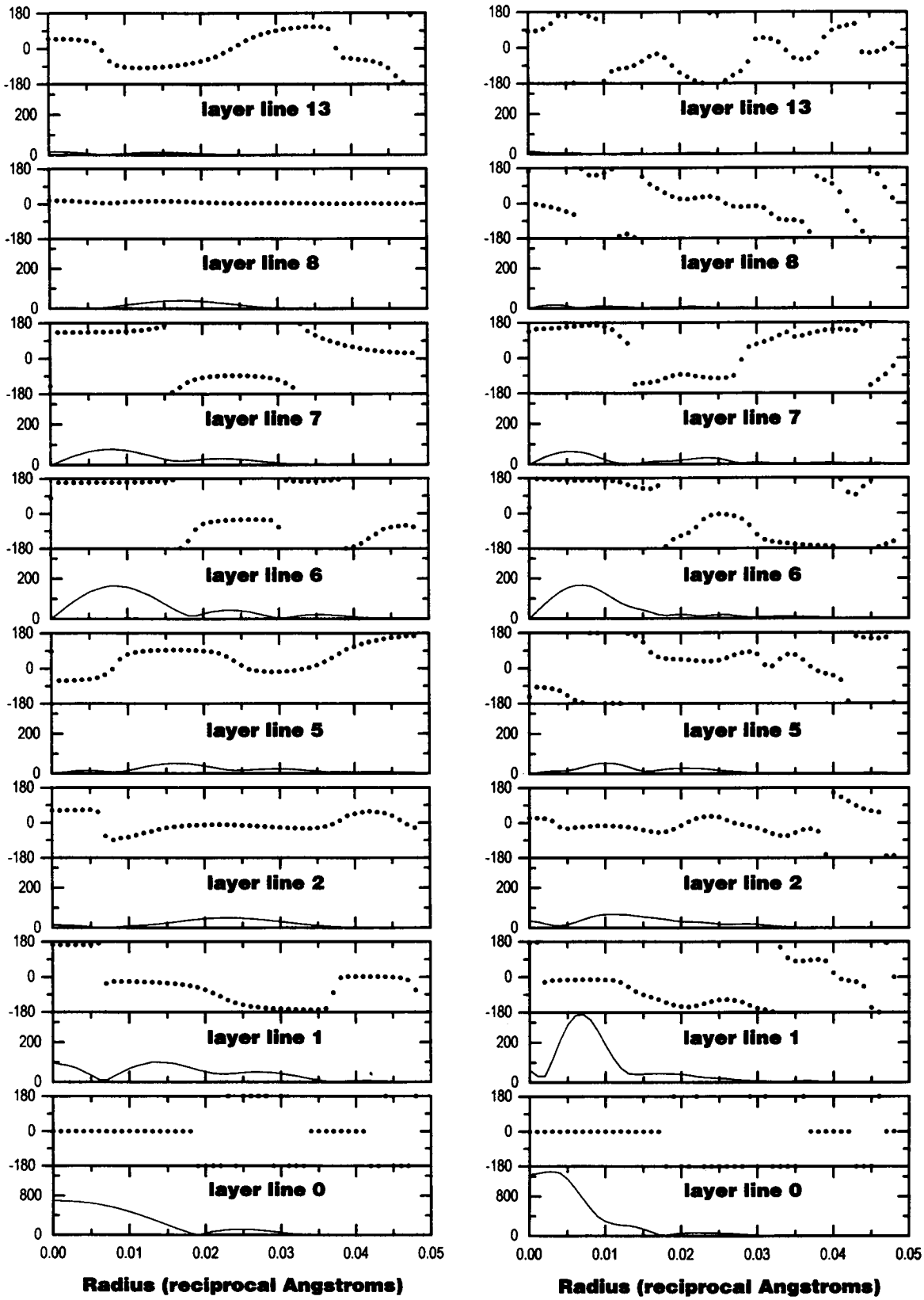

FIGURE 3 The averaged layer lines from the control erythrosin-phalloidin-actin filaments (*left*), and from the Fab-decorated filaments (*right*). The equators ($l = 0$, $n = 0$) are shown on a different scale. There is a large increase in intensity on the first actin layer line for the Fab-decorated filaments, and the peak moves in closer to the meridian, consistent with the contrast arising from a higher radius. The data sets for both the control and Fab-decorated filaments are each from 18 filaments (36 independent near-far data sets in each average).

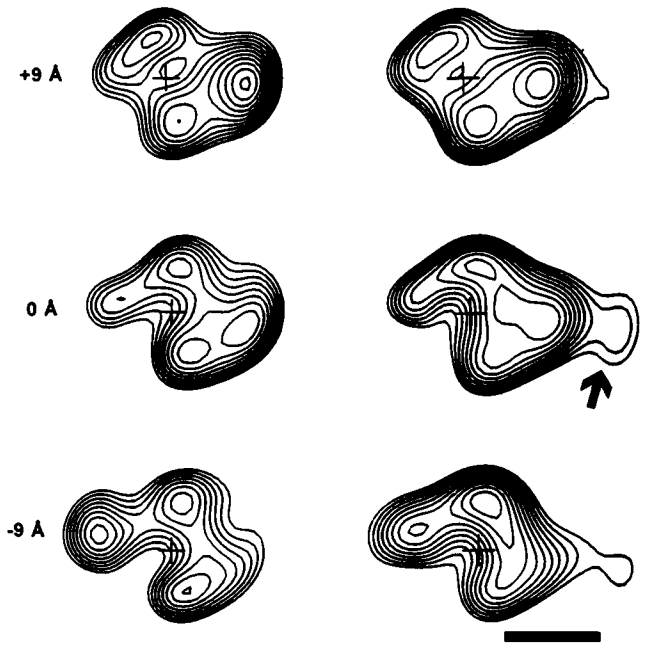

FIGURE 4 The layer lines of Fig. 3 have been used to generate a three-dimensional reconstruction. Three sections are shown for the control erythrosin-phalloidin-actin filaments (*a*) and from the Fab-decorated filaments (*b*). A + marks the position of the helical axis in each section. Sections are spaced axially by 9 Å. Because of the helical symmetry of actin, the section at +18 Å would be identical with the section at −9 Å, but rotated by 167°. The axial position of the origin (the section labeled *0 Å*) is arbitrary. The outer surface has been chosen so that the mass from the Fab fragment is seen (*arrow*), and so that the area that is actin appears similar in both data sets. This results in an enclosed volume for the control filament that is approximately 167% of the expected molecular volume, and a volume for the actin-Fab complex that is ~195% of the expected actin volume, assuming a partial specific volume for protein of 0.75 cm^3/g. Because the Fab fragment is about 50,000 mol wt, and actin is about 42,000 mol wt, the Fab should appear as a larger mass than the actin if it were visualized completely. The correct molecular volume for actin would be enclosed by the fourth contour line shown, rather than the first. However, this "correct" threshold level shows almost no contribution of the antibody in the Fab-decorated map. The scale bar is 40 Å.

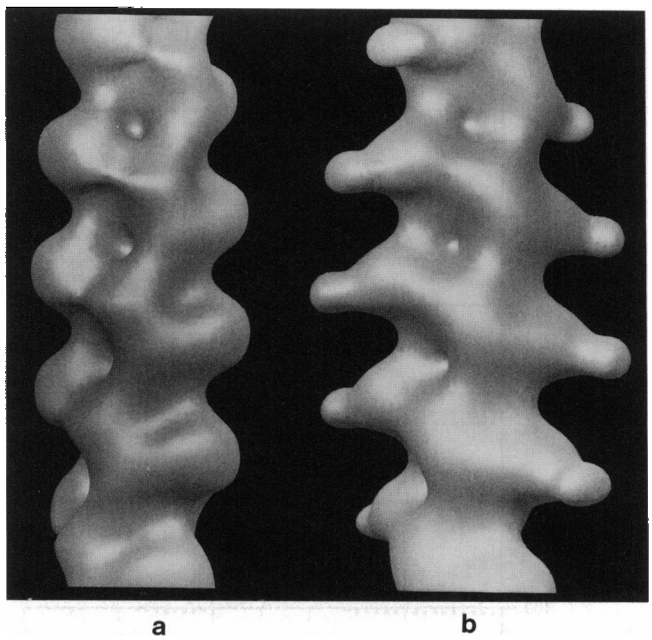

FIGURE 5 The surfaces of the three-dimensional reconstructions of the control erythrosin-phalloidin-actin filaments (*a*), and the Fab-decorated filaments (*b*). The same surface threshold densities have been used as in Fig. 4. With these thresholds, the two structures superimpose nearly identically everywhere except at the position of the antibody. The axial spacing between subunits along the same long-pitch helical strand is about 55 Å.

volume in the control actin reconstruction (Figs. 4*A* and 5*A*), the Fab density seen would correspond to only ~7% of 167% of the Fab volume.

We have also generated statistical difference maps (Egelman and Yu, 1989) between the control and the Fab-decorated filaments (Fig. 6). Such difference maps depend on first scaling the two maps, and we have used a least-squares procedure to find the multiplicative and additive constants to be applied to one map that minimize the differences with the second map. The difference peak due to the Fab fragment appears at 16 SD, and thus, not surprisingly, is highly significant. The difference maps show that the difference density due to the Fab fragment does not extend much further out in radius than what is shown by the outer contour in Fig. 4.

The simplest interpretation of the failure to visualize most of the Fab mass is that the Fab binding is quite disordered and does not have helical symmetry. Can this be due to specimen preparation for negatively stained electron microscopy? To test this, we have used cryo-electron microscopy of unstained, frozen-hydrated filaments. Fig. 7 shows a cryo-electron micrograph of actin filaments decorated with the Fab fragments. Although additional mass at high radius can be seen attached to the F-actin, one does not see the regular pattern of decoration that arises from the decoration of F-actin by myosin S-1. Thus, the raw micrographs of both negatively stained and frozen-hydrated filaments suggest that the binding is disordered. Fifteen filaments were selected that displayed symmetrical transforms with a clear first, second and sixth layer line. Averaging was performed as for the negatively stained filaments, and three filaments were rejected that did not average well. The resulting phase residuals were even worse than for negative stain (50° mean phase difference for the proper orientation, and 62° for the opposite orientation) suggesting that the signal to noise ratio is worse in ice, and also suggesting that the filaments are not better ordered in ice. The averaged layer lines from the frozen-hydrated filaments are shown in Fig. 8.

The large defocus that has been used for the frozen-hydrated images can, in principle, be corrected. The application of a Wiener filter requires an assessment of the signal to noise ratio as a function of resolution, and although this can be achieved for crystallographic material (Taylor and Crowther, 1992), it is more problematic for continuous data. We have chosen to use a simple weighting scheme for the

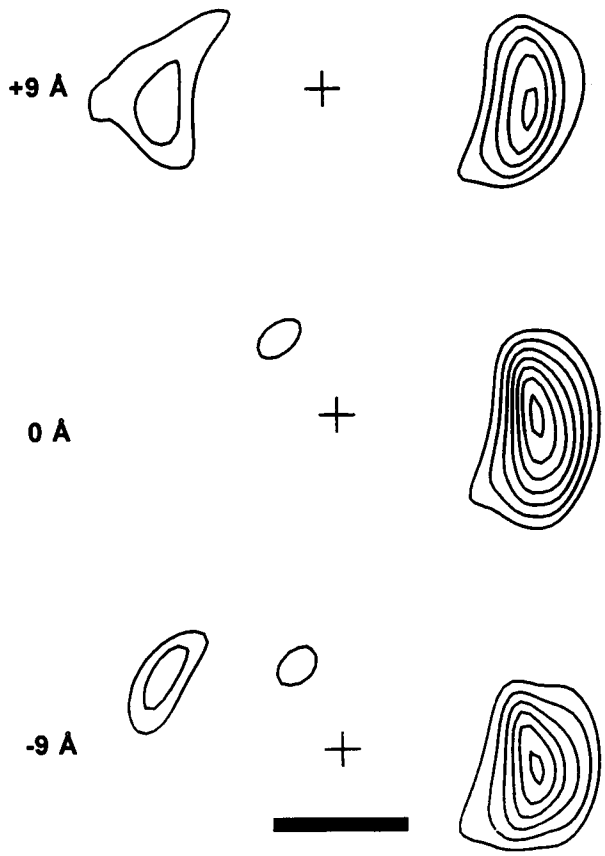

FIGURE 6 The statistical difference map, on which the differences are divided by the standard error of the differences, is shown for the actin-Fab and control actin maps. The first contour is at 4 SD with steps of 2 SD between contours. The peak difference, at 16 SD, is in the section at 0 Å. The positive contours are shown, in which a positive difference indicates that the actin-Fab map has a statistically significant greater density at a particular region than the control map. The Fab difference peak goes to zero at about 80 Å radius, indicating that there is no component of the averaged Fab density that exists at higher radius. There are no negative differences greater than 4 SD within a radius of 50 Å. The scale bar is 40 Å.

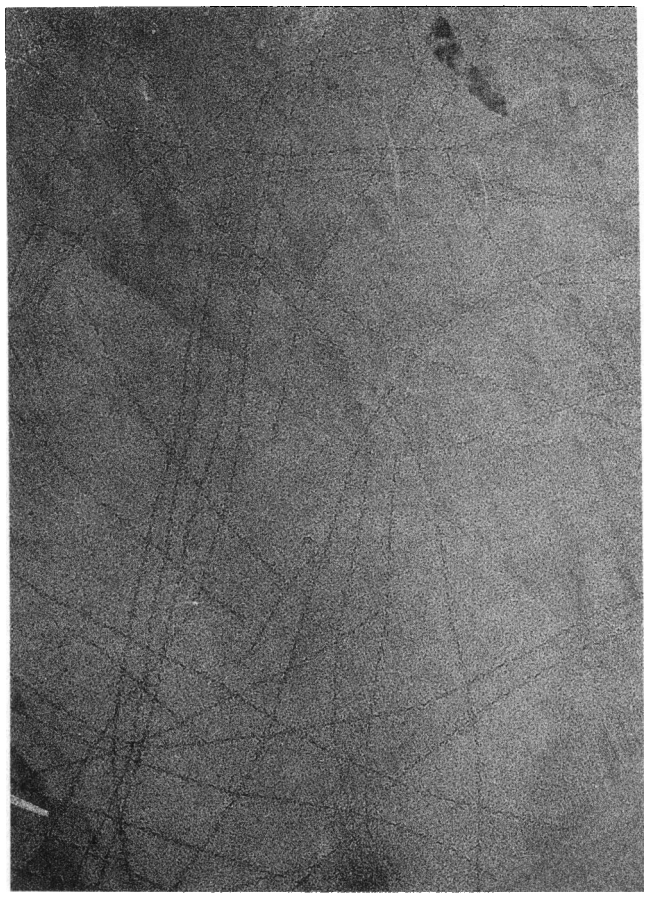

FIGURE 7 A cryo-electron micrograph of unstained, frozen-hydrated actin-Fab complexes. No regular decoration pattern can be seen, but additional mass can be observed bound to the actin filaments at irregular orientations. The frozen-hydrated images are consistent with the negatively stained images in showing that the Fab fragments bind in a disordered manner.

reconstruction in Fig. 9 in which the higher resolution components are corrected for the large falloff in intensity. This leads to a reconstruction that is more similar to both the negatively stained reconstruction and the atomic model of Holmes et al. (1990). However, the imposition of many different filter functions (or the use of uncorrected data) did not change the general feature of interest, the position and extent of the Fab mass in the reconstruction. The reconstruction in Fig. 9 has been shown with a surface containing approximately 195% of the molecular volume of actin, yet even at this level only a small portion of the antibody is visible. It can be seen that the location of the binding is in the same position as seen with the negatively stained filaments. As with the negatively stained filaments, no significant density appears at higher radius.

Given the general agreement between the negatively stained data and the frozen-hydrated, we have chosen to use the higher resolution negatively stained data for a comparison with the atomic model for F-actin (Fig. 10). This figure shows that the Fab mass in the reconstruction lies immediately adjacent to the position of the seven NH_2-terminal residues in the Holmes et al. (1990) model. The α-carbon atoms for residues 1–7 in the Holmes et al. model extend from 45 Å to 34 Å radius. Because the NH_2 terminus of actin is located near the helical axis in the model of Schutt et al. (1993), with the α-carbons for residues 1–7 running from 17 Å to 13 Å, this class of model is excluded by the data.

DISCUSSION

The most surprising feature of the reconstruction of the Fab-decorated actin is the failure to visualize most of the Fab mass. This could occur for four reasons: 1) the actual occupancy of the antibody is much lower than we imagined; 2) the distal portions of the antibody are highly disordered due to a large intrinsic flexibility in the Fab fragment; 3) the polyclonal antibodies that were used contain fragments that bind to actin with different orientations; and 4) the entire Fab is free to pivot about the binding site on F-actin, due to flexibility or disorder of the epitope.

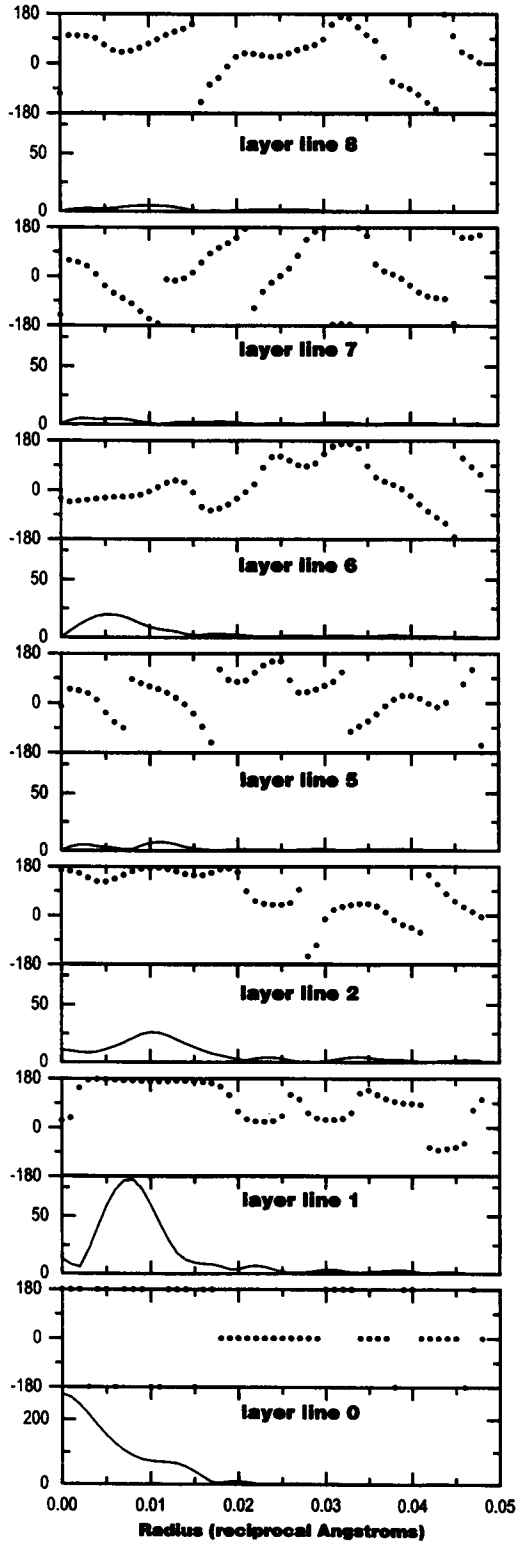

FIGURE 8 The averaged layer lines from frozen-hydrated actin-Fab filaments. Twelve filaments have been averaged (24 independent near-far data sets). As with the negatively stained specimens, there is a large intensity increase on the first layer line from the antibody binding. The position of the peak is also shifted in toward the meridian, as it is for the negatively stained Fab-decorated filaments.

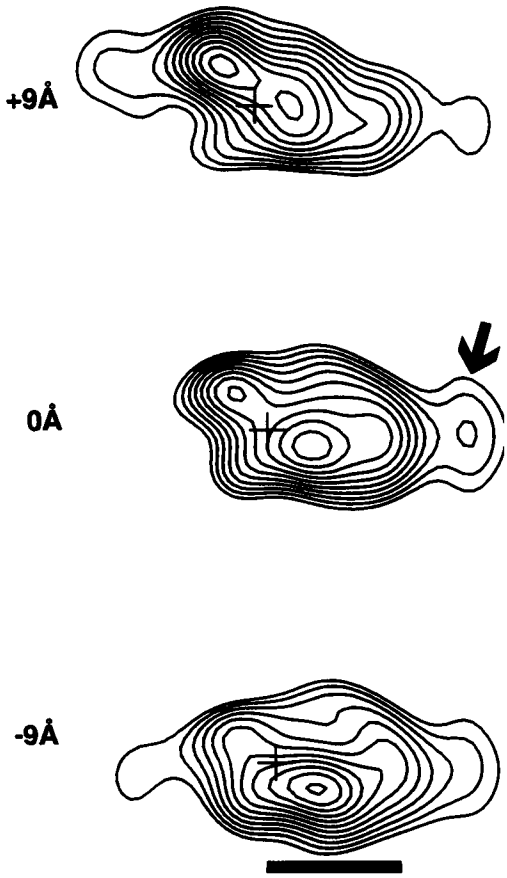

FIGURE 9 Three sections, with axial separations of 9 Å, for the unstained actin-Fab complex in ice. The layer lines of Fig. 8 have been used, with a weighting to compensate for the large defocus. The complex has the same orientation as the sections from the negatively stained reconstructions in Fig. 4. The arrow indicates the main mass of the Fab, seen in an position identical with that shown in Fig. 4 from negatively stained specimens. As with negative stain, most of the mass of the Fab is not visualized. The scale bar is 40 Å.

Inspection of the electron micrographs by eye suggests that the first possibility is unlikely; one can see that a large number of molecules apparently are bound to F-actin. Estimates of the occupancy from the binding constant also suggest that we are achieving at least an 80% occupancy. The statistical difference maps also show a difference between the control and Fab-decorated filaments centered at a radius of 60 Å, with this difference extending to 80 Å. If the Fab fragments were bound rigidly with a low occupancy, we would expect to see this difference extending to high radius. We therefore think that although we have less than complete occupancy, this will not have a major effect in explaining the failure to visualize most of the Fab mass. Three recent electron microscopic reconstructions of Fab fragments bound to viruses have shown nearly the full volume expected for the Fab (Prasad et al., 1990; Smith et al., 1993; Wang et al., 1992). On the other hand, Prasad et al. (1990) observed two different conformations of the Fab fragments within their reconstruction, suggesting that this involved two different bends between the variable and constant domains. This

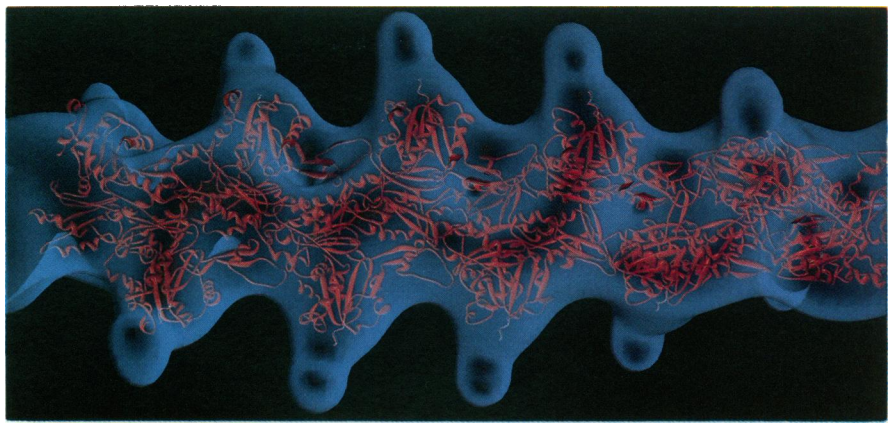

FIGURE 10 The transparent surface of the Fab-decorated actin filament (Fig. 5) is shown superimposed on a modified atomic model for F-actin (Holmes et al., 1990). The modification that we have made (Orlova and Egelman, 1992) involves a rotation of subdomain-2 of actin toward the filament axis by 15°. This results in a much better fit to electron microscopic reconstructions of either ADP-P_i actin or phalloidin-stabilized actin. The surface that is used contains 195% of the actin molecular volume, and it appears larger than the ribbon model because this volume does not include most of the Fab mass. The seven NH_2-terminal residues, the epitope for the Fab used, are shown in white. The density belonging to the Fab fragment appears clearly next to the seven residues in the model, excluding very different orientations of the actin monomer in the actin filament (Schutt et al., 1993).

would be consistent with an electron microscopic study (Wrigley et al., 1983) that directly visualized such variable bends, as well as a crystallographic study (Harris et al., 1992) in which two different elbow angles, differing by 16°, were seen. However, such variability within the switch region in the Fab cannot account for most of the disorder, because we would still expect to visualize more than half of the Fab, with only the most distal portions obliterated by the averaging.

The third possibility is a better candidate, because it is possible that some of the Fab fragments may be directed against residues 1–5, whereas others might be directed against residues 3–7. This could lead to a population of different orientations of the antibodies on F-actin. The fourth possibility, that the NH_2-terminal seven-residue epitope in F-actin is either disordered or quite flexible, is also attractive for several reasons. The acidic NH_2-terminal residues in actin form the most hydrophilic span in the actin sequence (Bulinski et al., 1983), and it is expected that these residues will be surrounded by solvent with minimal stabilization by the actin structure. In the G-actin-DNase I crystal the first six NH_2-terminal residues were described as having some of the highest temperature factors in the structure (Kabsch et al., 1990). A similarly large positional uncertainty was described for these residues in the actin-profilin crystal (Schutt et al., 1993). The NH_2 terminus in both crystals is in an irregular but helix-like conformation that is fully solvent accessible and not stabilized by interactions with any other part of the protein. Evidence for disorder in this region in the crystal supports our suggestion that these residues in F-actin are highly mobile. This has also been seen in an nuclear magnetic resonance study of a synthetic peptide containing actin residues 1–28, in which residues 1–4 were seen to be in a disordered helix-like state (Sonnichsen et al., 1992). However, the synthetic peptide study does not deal with the interactions between these residues and other parts of the molecule, such as the helix from 359 to 365, that might stabilize the NH_2 terminus.

Both the mobility of the NH_2 terminus and different orientations of polyclonal antibodies would explain why the observed Fab mass falls off rapidly with radius, because the binding site would be the fulcrum of a large lever arm. Thus, the further one travels from the binding site the less Fab mass would be helically averaged. Separating out the relative contributions of these two factors will require monoclonal antibodies to the NH_2 terminus.

Given the large disorder in the binding of the Fab fragments to actin, how can they reduce actin's internal torsional disorder? There are two possibilities: steric hindrance and induced conformational change. Steric hindrance would result from the prevention of large torsional motions due to the clash of antibodies bound to neighboring subunits along the same long-pitch helical strand. An induced conformational change would involve the binding of the antibody changing actin's structure in such a way that the internal dynamics are affected. The reduction in angular disorder, however, is much less than that generated by the rigor binding of myosin S-1 to actin (Stokes and DeRosier, 1987). One likely explanation for this effect is that myosin S-1 cross-bridges two actin monomers along the same long-pitch helical strand (Rayment et al., 1993), a possibility that is extremely unlikely for the Fab fragment.

Relation to myosin binding

The observations of DasGupta and Reisler (1989, 1991, 1992) on the effect of this Fab fragment on myosin S-1 binding to F-actin raise interest in the three-dimensional relation between the binding sites of the antibody and S-1 on actin. The main S-1 binding site lies on subdomain-1 of actin (Rayment et al., 1993), in which the NH_2 terminus is located. We show in Fig. 11 the geometry of acto-S-1 binding as determined by Milligan and Flicker (1987), in which it can be seen that the antibody binding site is located on a face of actin that is nearly perpendicular to the S-1 site. Thus, the

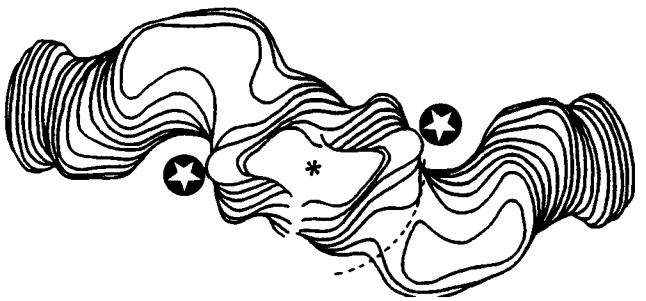

FIGURE 11 The reconstruction of acto-S-1 (Milligan, and Flicker, 1987) is shown, with the antibody location seen in our reconstruction indicated by the star. The geometry of the acto-S-1 rigor complex is very similar in the study of Rayment et al. (1993). The binding position that we observe, in the large cleft formed by the S-1 decoration, is consistent with the observed lack of a significant competition between the antibody binding and rigor S-1 binding. However, in the presence of nucleotide, DasGupta and Reisler (1989, 1991, 1992) observed a significant interference between antibody and S-1 binding.

antibody could easily bind in the large gaps present in an actin filament that has been fully decorated with S-1.

These observations need to be reconciled with the results of others who have studied the relation of the NH_2 terminus to myosin binding. Sutoh (1982, 1983) showed that actin residues 1–12 could be cross-linked to myosin subfragment-1, suggesting that these residues formed part of the rigor myosin binding site. However, the mobility of these residues and their proximity to the actual myosin binding site may explain the cross-linking result (Greene, 1984; Chen et al., 1985). Aspenstrom et al. (1991) showed that a mutant actin, in which the aspartic acids at positions 3 and 4 were changed to lysines, failed to bind myosin subfragment-1 in the absence of nucleotide (the rigor state). They concluded that residues 3 and 4 directly participate in the binding of myosin, but could not exclude the alternate possibility that mutations lead to secondary effects elsewhere in the actin structure. This alternate possibility now needs to be considered more seriously. An additional possibility is that the NH_2 terminus in the mutant actin is now shifted to a position that sterically blocks the rigor myosin binding site. This additional possibility, however, does not apply to the results of Sutoh et al. (1991) in which these same aspartic acids were mutated to histidines. They observed that the apparent affinity of actin and myosin in the presence of ATP was not changed, yet the maximum ATPase turnover rate dropped sharply. Similar results were obtained by Cook et al. (1992) who both mutated Asp-2 and Glu-4 to Asn-2 and Glu-4 to Gln-4, as well as deleted residues 2–4. In both of these modifications, they observed a significant drop in the actin-activated myosin ATPase. Interestingly, nearly opposite effects were observed by Cook et al. (1993) when two additional acidic residues were added to the NH_2 terminus of actin: the apparent affinity of actin and myosin in the presence of ATP was not affected, whereas the ATPase rate increased sharply. Together, these results suggest that the NH_2-terminal acidic residues play an important, but not clearly understood, role in the actomyosin ATPase.

We are still left with two structural possibilities: 1) the NH_2-terminal residues are not strongly involved in the rigor binding of myosin to actin, but are involved in the ATP-dependent binding, or 2) mutations or antibody binding to these residues induce an allosteric change in actin that can affect the actomyosin ATPase cycle, with or without a concomitant change in the rigor binding. Future experiments will be needed to distinguish between these possibilities.

We would like to thank Drs. Gargi DasGupta and Emil Reisler for the generous gift of the antibody, Dr. Ewa Prochniewicz for preparation of the labeled F-actin, and Dr. David Thomas for suggesting this project and for helpful discussions.

REFERENCES

Aspenstrom, P., and R. Karlsson. 1991. Interference with myosin subfragment-1 binding by site-directed mutagenesis of actin. *Eur. J. Biochem.* 200:35–41.

Bremer, A., R. C. Millonig, R. Sutterlin, A. Engel, T. D. Pollard, and U. Aebi. 1991. The structural basis for the intrinsic disorder of the actin filament: the "lateral slipping" model. *J. Cell Biol.* 115:689–703.

Bulinski, J. C., S. Kumar, K. Titani, and S. Hauschka. 1983. Peptide antibody specific for the amino terminus of skeletal muscle alpha-actin. *Proc. Natl. Acad. Sci., USA.* 80:1506–1510.

Chen, T., D. Applegate, and E. Reisler. 1985. Cross-linking of actin to myosin subfragment 1: course of reaction and stoichiometry of products. *Biochemistry.* 24:137–144.

Cook, R. K., W. T. Blake, and P. A. Rubenstein. 1992. Removal of the amino-terminal acidic residues of yeast actin. *J. Biol. Chem.* 267: 9430–9436.

Cook, R. K., D. Root, C. Miller, E. Reisler, and P. A. Rubenstein. 1993. Enhanced stimulation of myosin subfragment 1 ATPase activity by addition of negatively charged residues to the yeast actin NH_2 terminus. *J. Biol. Chem.* 268:2410–2415.

Craig, R., A. G. Szent-Gyorgi, L. Beese, P. Flicker, P. Vibert, and C. Cohen. 1980. Electron microscopy of thin filaments decorated with a Ca^{2+}-regulated myosin. *J. Mol. Biol.* 140:35–55.

DasGupta, G., and E. Reisler. 1989. Antibody against the amino terminus of α-actin inhibits actomyosin interactions in the presence of ATP. *J. Mol. Biol.* 207:833–836.

DasGupta, G., and E. Reisler. 1991. Nucleotide-induced changes in the interaction of myosin subfragment 1 with actin: detection by antibodies against the N-terminal segment of actin. *Biochemistry.* 30:9961–9966.

DasGupta, G., and E. Reisler. 1992. Actomyosin interactions in the presence of ATP and the N-terminal segment of actin. *Biochemistry.* 31: 1836–1841.

Egelman, E. H. 1986. An algorithm for straightening images of curved filamentous structures. *Ultramicroscopy.* 19:367–373.

Egelman, E. H., and D. J. DeRosier. 1992. Image analysis shows that variations in actin crossover spacings are random, not compensatory. *Biophys. J.* 63:1299–1305.

Egelman, E. H., and X. Yu. 1989. The location of DNA in RecA-DNA helical filaments. *Science (Washington DC).* 245:404–407.

Egelman, E. H., N. Francis, and D. J. DeRosier. 1982. F-actin is a helix with a random variable twist. *Nature (Lond.).* 298:131–135.

Greene, L. E. 1984. Stoichiometry of actin:S-1 cross-linked complex. *J. Biol. Chem.* 259:7363–7366.

Harris, L. J., S. B. Larson, K. W. Hasel, J. Day, A. Greenwood, and A. McPherson. 1992. The three-dimensional structure of an intact monoclonal antibody for canine lymphoma. *Nature (Lond.).* 360:369–372.

Herman, I. M. 1993. Actin isoforms. *Curr. Opinion Cell Biol.* 5:48–55.

Holmes, K. C., D. Popp, W. Gebhard, and W. Kabsch. 1990. Atomic model of the actin filament. *Nature (Lond.).* 347:44–49.

Kabsch, W., H. G. Mannherz, D. Suck, E. F. Pai, and H. C. Holmes. 1990. Atomic structure of the actin:DNase I complex. *Nature (Lond.).* 347: 37–44.

Miller, L., M. Kalnoski, Z. Yunossi, J. C. Bulinski, and E. Reisler. 1987. Antibodies directed against N-terminal residues on actin do not block acto-myosin binding. *Biochemistry*. 26:6064–6070.

Milligan, R. A., and P. F. Flicker. 1987. Structural relationships of actin, myosin, and tropomyosin revealed by cryo-electron microscopy. *J. Cell Biol.* 105:29–39.

Orlova, A., and E. H. Egelman. 1992. Structural basis for the destabilization of F-actin by phosphate release following ATP hydrolysis. *J. Mol. Biol.* 227:1043–1053.

Orlova, A., and E. H. Egelman. 1993. A Conformational change in the actin subunit can change the flexibility of the actin filament. *J. Mol. Biol.* 232:334–341.

Prasad, B. V., J. W. Burns, E. Marietta, M. K. Estes, and W. Chiu. 1990. Localization of VP4 neutralization sites in rotavirus by three-dimensional cryo-electron microscopy. *Nature (Lond.)*. 343:476–479.

Rayment, I., H. M. Holden, M. Whittaker, C. B. Yohn, M. Lorenz, K. C. Holmes, and R. A. Milligan. 1993. Structure of the actin-myosin complex and its implications for muscle contraction. *Science (Washington DC)*. 261:58–65.

Schutt, C. E., J. C. Myslik, M. D. Rozycki, N. C. W. Goonesekere, and U. Lindberg. 1993. The structure of crystalline profilin:β-actin. *Nature (Lond.). 365:810–816.*

Smith, T. J., N. H. Olson, R. H. Cheng, H. Liu, E. S. Chase, W. M. Lee, D. M. Leippe, A. G. Mosser, R. R. Rueckert, and T. S. Baker. 1993. Structure of human rhinovirus complexed with Fab fragments from a neutralizing antibody. *J. Virol.* 67:1148–1158.

Sonnichsen, F. D., J. E. Van Eyk, R. S. Hodges, and B. D. Sykes. 1992. Effect of trifluoroethanol on protein secondary structure: an NMR and CD study using a synthetic actin peptide. *Biochemistry*. 31:8790–8798.

Stokes, D. L., and D. J. DeRosier. 1987. The variable twist of actin and its modulation by actin-binding proteins. *J. Cell Biol.* 104:1005–1017.

Sutoh, K. 1982. Identification of myosin-binding sites on the actin sequence. *Biochemistry*. 21:3654–3661.

Sutoh, K. 1983. Mapping of actin-binding sites on the heavy chain of myosin subfragment 1. *Biochemistry*. 22:1579–1585.

Sutoh, K., M. Ando, and Y. Y. Toyoshima. 1991. Site-directed mutations of Dictyostelium actin: Disruption of a negative charge cluster at the N terminus. *Proc. Natl. Acad. Sci. USA*. 88:7711–7714.

Taylor, K. A., and R. A. Crowther. 1992. 3D reconstruction from the Fourier transform of a single superlattice image of an oblique section. *Ultramicroscopy*. 41:153–167.

Wang, G. J., C. Porta, Z. G. Chen, T. S. Baker, and J. E. Johnson. 1992. Identification of a Fab interaction footprint site on an icosahedral virus by cryoelectron microscopy and x-ray crystallography. *Nature (Lond.)*. 355:275–278.

Wrigley, N. G., E. B. Brown, and J. J. Skehel. 1983. Electron microscopic evidence for the axial rotation and inter-domain flexibility of the Fab regions of Immunoglobulin G. *J. Mol. Biol.* 169:771–774.